The Effect of Estimated Headway on Gradient Highway by Means of Linear and Nonlinear Stability

S. Jin[a,*] and Z.-C. Liu[b]

[a] *School of Information Science and Engineering, Chongqing Jiaotong University, Chongqing 400074, China*
[b] *College of Artificial Intelligence, Chongqing Technology and Business University, Chongqing 400067, China*

Received: 15.12.2022 & Accepted: 27.04.2023

Doi: 10.12693/APhysPolA.144.15 *e-mail: jsfj@cqjtu.edu.cn

An extended car-following model is presented in this paper, which considers both gradient and estimated headway. The study analyzes the impact of these factors on traffic flow stability using linear stability theory and the nonlinear reductive perturbation method. Numerical simulation reveals that the kink–antikink solution of the modified Korteweg–de Vries equation can describe the propagating behavior of traffic density waves near critical points. Furthermore, considering estimated headway information enhances traffic flow stability on both slope roads and flat roads, indicating its crucial role in alleviating congestion.

topics: car-following model, gradient road, traffic flow, estimated effect of driver

1. Introduction

As one of the most important environmental factors for vehicle driving, roads directly determine the performance of vehicles and the difficulty level of completing driving tasks. Due to topographical fluctuations and urban three-dimensional transportation systems, undulating roads have become one of the more common working conditions in daily driving processes. Therefore, the impact of road slopes on vehicle driving has become a research hotspot [1, 2]. Research has found that sags (where the slope varies significantly from downhill to uphill) can induce undesired traffic instability and capacity drop and, therefore, worsen traffic congestion and throughput [3]. As is well known, traffic flow research has been conducted for decades to better understand the phenomenon and its characteristics. Scholars have proposed various models, including macroscopic [4–13], mesoscopic [14–17], and microscopic models [18–24]. The car-following model is a commonly used microscopic model that describes traffic flow. Bando et al. [17] proposed an optimal velocity model to study the dynamic behavior of traffic flow. On this basis, Helbing et al. [18] found that the acceleration and deceleration values of the optimal speed model differed greatly from the values obtained in an actual situation through measurement, so they proposed a generalized force model [18]. Moreover, to analyze the impact of time delay and the kinematic wave velocity, Jiang et al. [9] proposed a full velocity difference model (FVDM).

The current research on car-following theory is impressive, but it has mainly focused on simple road scenes without considering the slope and other road characteristics. Consequently, researchers have explored traffic flow behaviors on sloped roads. Li et al. [20] investigated the phase transition of traffic flow considering speed limits in gradient scenarios. Meanwhile, Komada et al. [21] examined how gravity affects traffic flow under sloped roads. Zhu and Yu [22] analyzed traffic flow characteristics, including road slope. Meng and Yan [23] developed a new model for traffic flow on curved roads with slopes. Sun et al. [24] investigated the impact of driver characteristics on traffic stability on gradient highways, finding that aggressive drivers stabilize flow while timid drivers destabilize it, regardless of uphill or downhill direction. To capture the effects of sloping roads, this study proposed a generic approach to extend any (free-flow or car-following) microscopic models characterized by acceleration functions [25]. Considering that the performance of various types of vehicles is multifarious and the vehicles sometimes drive on the road with slopes, a novel two-lane lattice hydrodynamic model on a gradient road considering heterogeneous traffic

flow was proposed [26]. Zhang et al. [7] deduced a macroscopic traffic model on the uphill and downhill slopes by employing the transformation relation of microscopic variables to macroscopic ones based on a microscopic car-following model considering the velocity difference between adjacent vehicles.

A new continuum model was proposed by Zhai et al. [27] to account for the velocity uncertainty of preceding vehicles on gradient highways, and showed that slope information and uncertainty have significant impacts on traffic congestion and energy consumption. Specifically, slope information has a positive effect, while uncertainty has a negative effect. Wang et al. [28] developed an extended macro model for single-lane systems that considers the dynamic effects of electronic throttle and analyzes the complex influence of road geometry on traffic flow stability. Zhang et al. [29] developed a macroscopic traffic model for uphill and downhill slopes by transforming microscopic variables to macroscopic ones using a car-following model that considers the velocity difference between adjacent vehicles. Han et al. [30] studied car-following behavior, taking into account the driver, vehicle, and environment. Lee et al. [31] proposed an eco-driving strategy to reduce energy consumption in various driving situations, including road slopes and car-following scenarios. Additionally, several other studies have investigated vehicle behavior on gradient highways [32–36].

We propose a new car-following model that considers the estimated headway on gradient highways. This is important because in slope road scenarios, the speed of the front vehicle changes frequently, which should be taken into account when estimating its effect. However, previous works have not considered the estimated effect of slope roads. Using our proposed model, we analyzed both linear and nonlinear stability and explored how estimated driving behavior on gradients affects traffic congestion. We also revealed how the estimated headway influences the spatial-temporal evolution characteristics of traffic flow. Our simulation results demonstrate the effectiveness of this method.

This paper is organized as follows. Sect. 1 provides an introduction to relevant works. In Sect. 2, we propose a new car-following model that considers estimated headway on gradient highways. We conduct a linear stability analysis of the proposed model in Sect. 3. Nonlinear stability analysis of the proposed model is conducted in Sect. 4. In Sect. 5, we present and analyze interesting results from numerical simulations. Finally, conclusions and future work are discussed in Sect. 6.

2. Model considering gradient and estimated headway

First, we consider that vehicles move ahead on a single-lane gradient highway, as described in Fig. 1.

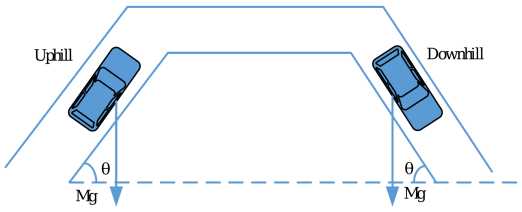

Fig. 1. Schematic diagram of vehicle driving on gradient highway.

In Fig. 1, θ represents the slope, g represents the gravitational acceleration, and M denotes the mass of the vehicle. According to Newton's theorem of mechanics, the dynamic equation for vehicles traveling on slope roads is

$$M\frac{\mathrm{d}^2x_m(t)}{\mathrm{d}t^2} = F\big(\Delta x_m(t)\big) - \mu\frac{\mathrm{d}x_m(t)}{\mathrm{d}t} - Mg\sin(\theta)B\big(\Delta x_m(t)\big), \tag{1}$$

where $x_m(t)$ represents the position of vehicle m at time t, the $\Delta x_m(t) = x_{m+1}(t) - x_m(t)$ is the headway of vehicle m at time t. In (1), $F(\Delta x_m(t))$ indicates the driving force of the vehicle, and μ is the friction coefficient. The braking control function $B(\Delta x_m(t))$ represents a function of the shop distance $x_m(t)$, while $F(\Delta x_m(t))$ is a linear function about $x_m(t)$, namely,

$$F(\Delta x_m(t)) = \alpha F\big(\Delta x_m(t)\big). \tag{2}$$

Here, α is a constant of proportionality. Further, (2) can be rewritten as follows

$$\frac{\mathrm{d}^2x_m(t)}{\mathrm{d}t^2} = -\frac{\mu}{M}\frac{\mathrm{d}x_m(t)}{\mathrm{d}t} + \frac{\mu}{M}\left[\frac{\alpha F(\Delta x_m(t))}{\mu} - \frac{Mg\sin(\theta)B(\Delta x_m(t))}{\mu}\right]. \tag{3}$$

According to the literature [19], the optimal velocity car-following model is

$$\frac{\mathrm{d}^2x_m(t)}{\mathrm{d}t^2} = a\left[V(\Delta x_m(t)) - \frac{\mathrm{d}x_m(t)}{\mathrm{d}t}\right]. \tag{4}$$

The optimal velocity function is

$$V(\Delta x_m(t)) = v_{f,\max}\frac{\tanh(\Delta x_m(t)-h_c)+\tanh(h_c)}{2}, \tag{5}$$

where $a = 1/\tau$ is the driver's sensitivity coefficient and τ is the delay time, $v_{f,\max}$ denotes the maximum speed of the vehicle when the road has no slope. It is worth noting that the optimal velocity function mentioned here indicates that the optimal velocity of the following vehicle m depends on the headway $\Delta x_m(t)$ between the following vehicle m and the preceding vehicle $m+1$. When $\Delta x_m(t) \to 0$, the optimal velocity $V(\Delta x_m(t)) \to 0$, thus avoiding collisions. When the $\Delta x_m(t) \to \infty$, the optimal velocity $V(\Delta x_m(t)) \to v_{f,\max}$, indicating that the vehicle is in a free-flowing state. Here we can consider $\Delta x_m(t)$ as the cost function.

When $\theta = 0$, then (1) and (3) are equivalent, and we have

$$\frac{\alpha F\big(\Delta x_m(t)\big)}{\mu} = v_{f,\max}\,\frac{\tanh(\Delta x_m(t)-h_c)+\tanh(h_c)}{2} \tag{6}$$

and $\mu/M = a$. As shown in the literature [21],

$$\frac{Mg\sin(\theta)B(\Delta x_m(t))}{\mu} = v_{g,\max}\,\frac{\tanh(\Delta x_m(t)-h_b)+\tanh(h_b)}{2}, \tag{7}$$

where $v_{g,\max} = Mg\sin(\theta)/\mu$, h_b denotes the braking distance, and $v_{g,\max}$ and $\sin(\theta)$ are proportional to each other. Therefore, considering the effect of slope, the expression of the optimal velocity function of the vehicle when driving uphill is obtained as follows

$$V(\Delta x_m(t)) = v_{f,\max}\,\frac{\tanh(\Delta x_m(t)-h_c)+\tanh(h_c)}{2} - v_{g,u,\max}\,\frac{\tanh(\Delta x_m(t)-h_{b,u})+\tanh(h_{b,u})}{2}. \tag{8}$$

The expression for the optimal velocity function of the vehicle while driving downhill is

$$V(\Delta x_m(t)) = v_{f,\max}\,\frac{\tanh(\Delta x_m(t)-h_c)+\tanh(h_c)}{2} + v_{g,d,\max}\,\frac{\tanh(\Delta x_m(t)-h_{b,d})+\tanh(h_{b,d})}{2}, \tag{9}$$

where h_c is the safe distance of the vehicle on the plane road, $h_{b,u}$ represent the safe distance for an uphill gradient highway, $h_{b,d}$ represent the safe distance for a downhill gradient highway. On a slope road, the safety distance between vehicles is related to the slope of the road. Therefore, we use $h_{c,\theta}$ instead of $h_{b,u}$ and $h_{b,d}$, as can be seen in literature [19], where $h_{c,\theta} = h_c\,(1+\eta\sin(\theta))$ for downhill slope and $h_{c,\theta} = h_c\,(1-\xi\sin(\theta))$ for uphill slope. In general, we assume that $\xi = \eta = 1$. Note that $v_{g,d,\max}$ and $v_{g,u,\max}$ are the maximal reduced and enhanced velocity on uphill and downhill gradients and the expression is $v_{g,d,\max} = v_{g,u,\max} = v_{g,\max}$; when $\theta = 0$, then $v_{g,\max} = 0$. Therefore, based on the above analysis, we can obtain the car-following model on the slope scenario as

$$\frac{\mathrm{d}^2x_m(t)}{\mathrm{d}t^2} = a\left[V(\Delta x_m(t)) - \frac{\mathrm{d}x_m(t)}{\mathrm{d}t}\right]. \tag{10}$$

The expression of the optimal velocity function in (10) is

$$V(\Delta x_m(t)) = \frac{v_{f,\max}\pm v_{g,\max}}{2} \times\Big[\tanh(\Delta x_m(t)-h_{c,\theta})+\tanh(h_{c,\theta})\Big] = \frac{v_{f,\max}\pm v_{g,\max}}{2}\,V_s(\Delta x_m(t)), \tag{11}$$

where $V_s(\Delta x_m(t)) = \tanh(\Delta x_m(t)-h_{c,\theta}) + \tanh(h_{c,\theta})$, the sign "+" indicates the situation when the vehicle is on a downhill slope and the sign "-" indicates the situation when the vehicle is on an uphill slope.

Now, (11) can be rewritten as

$$\frac{\mathrm{d}^2x_m(t)}{\mathrm{d}t^2} = a\left[\frac{v_{f,\max}\pm v_{g,\max}}{2}V_s(\Delta x_m(t)) - \frac{dx_m(t)}{\mathrm{d}t}\right]. \tag{12}$$

The speed of the car in front is constantly changing, especially on a sloped road. To adjust the speed of the vehicle accordingly, it is necessary to predict the future disturbance distance between the front and rear vehicles based on their current speeds. More specifically, when the vehicle adjusts its speed according to the headway, the headway will also change due to the change in the speed of the preceding vehicle, and the changed headway is the future disturbance distance. This allows for real-time dynamic micro adjustments to maintain the optimal speed of the vehicle. We propose a car-following model that considers estimated headway based on (12). The evolution differential equation is as follows

$$\frac{\mathrm{d}^2x_m(t)}{\mathrm{d}t^2} = a\Big[\frac{v_{f,\max}\pm v_{g,\max}}{2}\,V_s\big(\Delta x_m(t)+T\Delta v_m(t)\big) - \frac{\mathrm{d}x_m(t)}{\mathrm{d}t}\Big], \tag{13}$$

where the T is the predicted time, $T\Delta v_m(t)$ represents the estimated headway; when $T = 0$, the equation (13) will degenerate into (10). If $V_s(\Delta x_m(t) + T\Delta v_m(t))$ in the model is expanded according to the Taylor series, and the nonlinear term above the second order is omitted, we obtain

$$V_s(\Delta x_m(t) + T\Delta v_m(t)) = V_s(\Delta x_m(t)) + V_s'(\Delta x_m(t))\,T\Delta v_m(t). \tag{14}$$

Then we have

$$\frac{\mathrm{d}^2x_m(t)}{\mathrm{d}t^2} = a\Big[q\,V_s(\Delta x_m(t)) + q\,V'_s(\Delta x_m(t))\,T\Delta v_m(t) - \frac{\mathrm{d}x_m(t)}{\mathrm{d}t}\Big], \tag{15}$$

where $V_s'(\Delta x_m(t)) = \frac{\mathrm{d}V_s(\Delta x_m(t))}{\mathrm{d}\Delta x_m(t)}$, $q = \frac{v_{f,\max}\pm v_{g,\max}}{2}$. In order to facilitate the subsequent analysis, we write (15) in the form of difference, and the specific form is as follows

$$\begin{aligned}\Delta x_m(t+2\tau) &= \Delta x_m(t+\tau)\\ &+\tau q\big[V_s(\Delta x_{m+1}(t)) - V_s(\Delta x_m(t))\big]\\ &+Tq\big[V_s'(\Delta x_{m+1}(t)) - V_s'(\Delta x_m(t))\big]\\ &\times(\Delta x_{m+1}(t+\tau) - \Delta x_{m+1}(t))\\ &+TqV_s'(\Delta x_m(t))\Big(\Delta x_{m+1}(t+\tau)\\ &-\Delta x_{m+1}(t) - \Delta x_m(t+\tau) + \Delta x_m(t)\Big).\end{aligned} \tag{16}$$

3. Linear stability analysis

Linear stability analysis helps to investigate how estimated headway and slope affect traffic flow. Assuming an initial equilibrium state, all vehicles have a headway of h, and the corresponding optimized speed is $(\frac{v_{f,\max}\pm v_{g,\max}}{2})\,V_s(h)$, at this time, the positions of all vehicles in steady-state traffic flow are

$$x_m^{(0)}(t) = hn + \frac{v_{f,\max} \pm v_{g,\max}}{2}\, V_s(h),$$
$$h = L/N, \tag{17}$$

where L represents the length of the road, and N is the number of vehicles studied. Adding the disturbance $y_m(t)$ to the uniform flow (17), we can obtain

$$x_m(t) = {x_m}^{(0)}(t) + y_m(t). \tag{18}$$

Taking (18) into difference (16) and linearizing it, we can get

$$\begin{aligned}\Delta y_m(t+2\tau) &= \Delta y_m(t+\tau)\\ &+\tau q {V_s}'\left[\Delta y_{m+1}(t) - \Delta y_m(t)\right]\\ &+Tq{V_s}'\Big[\Delta y_{m+1}(t+\tau) - \Delta y_{m+1}(t)\\ &-\Delta y_m(t+\tau) + \Delta y_m(t)\Big],\end{aligned} \tag{19}$$

where $\Delta y_m(t) = y_{m+1}(t) - y_m(t)$, ${V_s}' = \frac{\mathrm{d}V_s(\Delta x_m(t))}{\mathrm{d}\Delta x_m(t)}\big|_{\Delta x_m(t)=h}$. Let $\Delta y_m(t) = \mathrm{e}^{\mathrm{i}km+zt}$, expand (19) according to the Fourier series to get

$$\begin{aligned}&\mathrm{e}^{2z\tau} - \mathrm{e}^{z\tau} - \tau q {V_s}'\left(\mathrm{e}^{\mathrm{i}k} - 1\right)\\ &-Tq{V_s}'\left[\left(\mathrm{e}^{\mathrm{i}k} - 1\right)\left(\mathrm{e}^{z\tau} - 1\right)\right] = 0.\end{aligned} \tag{20}$$

Expanding the parameter z into $z = z_1(\mathrm{i}k) + z_2(\mathrm{i}k)^2 + \ldots$, by omitting the terms above the second order, we can get

$$z_1 = \frac{v_{f,\max} \pm v_{g,\max}}{2}\, V_s', \tag{21}$$

$$z_2 = \frac{1}{2} q {V_s}'\left[1 + 2Tq{V_s}' - 3\tau q {V_s}'\right]. \tag{22}$$

The system's behavior depends on the sign of z_2. If $z_2 > 0$, the traffic flow will evolve from an initial equilibrium state to an unstable state, causing the magnitude of the disturbance to increase over time until it reaches a stop-and-go traffic congestion phenomenon. On the other hand, if $z_2 < 0$, the traffic flow will return to a stable state under initial disturbance. Therefore, we can obtain the critical stability condition for traffic flow as follows

$$\tau = \frac{1 + 2T\left(\frac{v_{f,\max}\pm v_{g,\max}}{2}\right)\, {V_s}'}{3\left(\frac{v_{f,\max}\pm v_{g,\max}}{2}\right)\, {V_s}'}. \tag{23}$$

Take $v_{f,\max} = 2$, $\frac{mg}{\mu} = 1$, we get

$$\tau = \frac{2 + 2T\left(2 \pm \sin(\theta)\right)\, {V_s}'}{3\left(2 \pm \sin(\theta)\right)\, {V_s}'}. \tag{24}$$

For small disturbances in the long-wave mode, the traffic flow will remain stable when the headway meets the following condition

$$\tau < \frac{2 + 2T\left(2 \pm \sin(\theta)\right)\, {V_s}'}{3\left(2 \pm \sin(\theta)\right)\, {V_s}'}; \tag{25}$$

when parameter $T = 0$, parameter $\theta = 0$, we can get the stable condition

$$\tau < \frac{1}{3{V_s}'}. \tag{26}$$

The estimated headway T and the angle of slope both affect the stability of the car-following model, as shown in (25). Figure 2 displays stable phase diagrams for different values of T and θ on uphill,

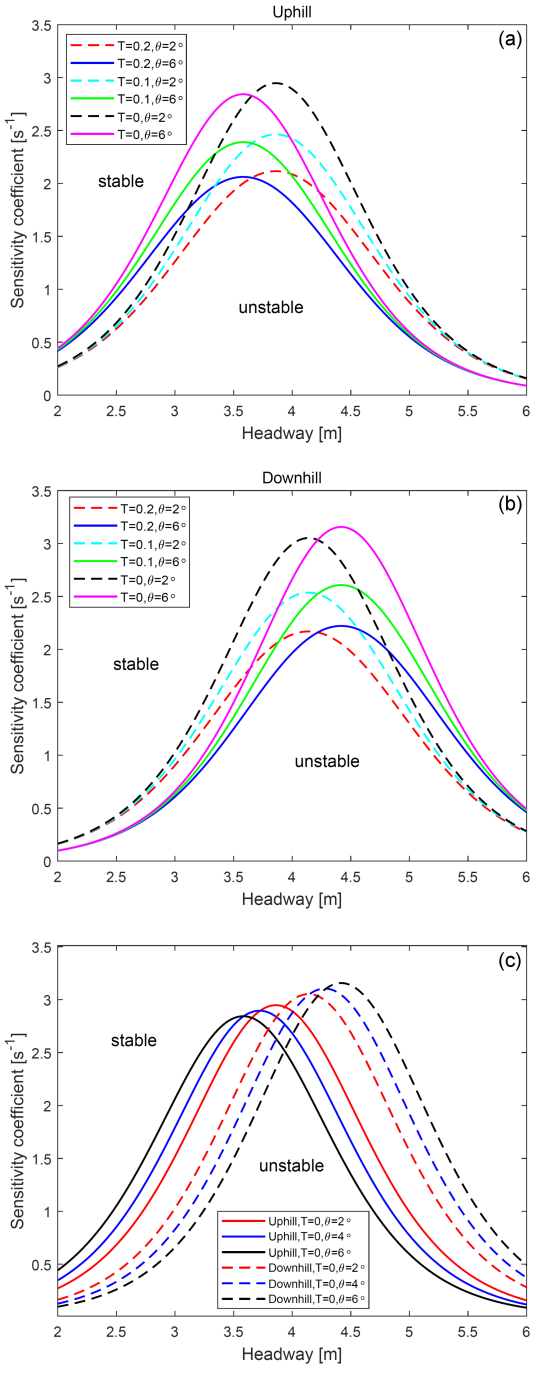

Fig. 2. Stable phase diagram for different values of T and θ (uphill and downhill slopes).

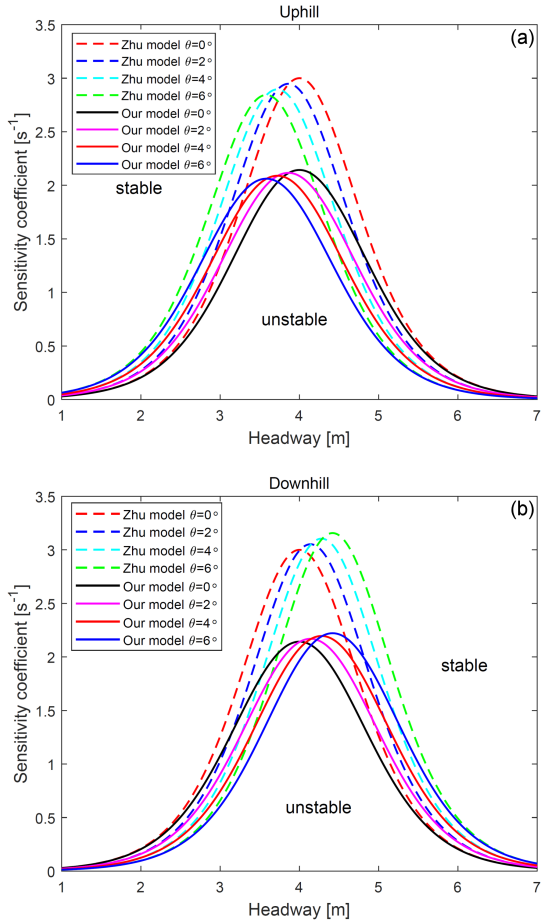

Fig. 3. Stable phase diagram for different models (uphill and downhill slopes).

downhill, and flat roads. In Fig. 2a, all lines represent critical stability curves; regions above these lines are stable, while those below are unstable. Fig. 2a shows the stability curves for uphill angles of $\theta = 6°$ and $2°$, with solid and dashed lines, respectively. The values of T are 0.2, 0.1, and 0 for both cases. The figure indicates that a larger T results in a larger stability area and smaller impact range for the same uphill angle case. When $T = 0.2$, the stability area for an uphill angle of $\theta = 6°$ is larger than that for $\theta = 2°$. This suggests that a steeper uphill angle leads to more favorable traffic flow stabilization, which aligns with previous research [21]. Figure 2b shows the stability curve for three different T values at a downhill angle of $\theta = 6°$ represented by a solid line. The dashed lines represent the stability curves for $\theta = 2°$ with T values of 0.2, 0.1, and 0, respectively. A larger T results in a larger stability area for the model at the same downhill angle. However, when comparing models with equal T, such as $T = 0.1$, the stability area is smaller for $\theta = 6°$ than it is for $\theta = 2°$. This suggests that traffic stabilization improves as the downhill angle decreases; this conclusion has also been found in previous literature [24]. To more clearly compare the stability of uphill and downhill slopes at varying angles, Fig. 2c gives the stability curves of uphill and downhill slopes at angles of $\theta = 2°$, $\theta = 4°$, and $\theta = 6°$ for $T = 0$, respectively. The solid line indicates the uphill case, and the dashed line indicates the downhill case. It is obvious that the stability regions of the corresponding curves for the uphill slope are larger than those for the downhill slope. In addition, in all the solid lines, the higher the uphill angle, the shorter the apex of the curve. In all the dashed lines, the higher the downhill angle, the higher the apex of the curve.

To highlight the advantages of the proposed model in this paper, we compare the phase stability curves of the model in [22] (referred to as the Zhu model) and the model in this paper. Figure 3a shows the phase stability curves of the two models for different slope angles ($\theta = 0°$, $\theta = 2°$, $\theta = 4°$ and $\theta = 6°$) in the uphill case. The solid line represents the Zhu model [22], and the dashed line represents our model. It is obvious from the figure that the curve stability regions of our model are larger than those of the Zhu model for all four slope angle cases. Figure 3b represents the phase stability curves of the two models at different slope angles in the downhill case. Similarly, in the downhill case, the curve stabilization area of our model is larger than that of the Zhu model for all four slope angle cases. It can be seen that considering the estimated headway in the model from this paper is beneficial to the traffic stabilization of sloped roads.

4. Nonlinear stability analysis

Based on the results of linear stability analysis, the nonlinear analysis of the traffic characteristics of the proposed model near the critical point (h_c, a_c) is carried out by using the perturbation analysis method, which can reveal the influence of the estimated headway on the spatial-temporal evolution characteristics of traffic flow. First, near the critical point (h_c, a_c), for a given small parameter $\varepsilon(0 < \varepsilon \ll 1)$, for space variables m and time variables t, we define the corresponding space slow variables X and time slow variables T as follows

$$X = \varepsilon\,(m + bt)\,, \quad T = \varepsilon^3 t, \tag{27}$$

where parameter b is undetermined constant. Let $\Delta x_m(t)$ satisfy

$$\Delta x_m(t) = h_c + \varepsilon R(X, T). \tag{28}$$

By substituting (27) and (28) into (16), and expanding (16) to the Taylor series ε^5, we get the following partial differential equation

$$\begin{aligned} &\varepsilon^2 \Sigma_1 \partial_X R + \varepsilon^3 \Sigma_2 \partial_X^2 R \\ &+\varepsilon^4 \left(\Sigma_3 \partial_X^3 R - \Sigma_4 \partial_X R^3 + \partial_T R\right) \\ &+\varepsilon^5 \left(\Sigma_5 \partial_X^4 R - \Sigma_6 \partial_X^2 R^3 + \Sigma_7 \partial_T \partial_X R\right) = 0, \end{aligned} \tag{29}$$

where

$$\begin{aligned}
&\Sigma_1 = b - qV_s'(h_c),\\
&\Sigma_2 = \tfrac{3}{2}b^2\tau - \tfrac{1}{2}qV_s'(h_c) - TqV_s'(h_c)b,\\
&\Sigma_3 = b^3\tau^2 - \tfrac{1}{6}qV_s'(h_c) - \tfrac{1}{2}TqV_s'(h_c)\left(b + b^2\tau\right),\\
&\Sigma_4 = \tfrac{1}{6}qV_s'''(h_c),\\
&\Sigma_5 = \tfrac{1}{4}b^4\tau^3 - \tfrac{1}{24}qV_s'(h_c) - \tfrac{1}{6}bTqV_s'(h_c)\\
&\quad -\tfrac{1}{4}TqV_s'(h_c)b^2\tau, \Sigma_6 = \tfrac{1}{12}qV_s'''(h_c),\\
&\Sigma_7 = 3b\tau - TqV_s'(h_c),
\end{aligned} \tag{30}$$

and $\partial_X = \frac{\partial}{\partial X}$, $\partial_T = \frac{\partial}{\partial T}$, $\partial_T\partial_X = \frac{\partial^2}{\partial T \partial X}$, while

$$\begin{aligned}
&V_s'(h_c) = \left.\frac{\mathrm{d}V_s(\Delta x_m(t))}{\mathrm{d}\Delta x_m(t)}\right|_{\Delta x_m(t)=h_c},\\
&V_s'''(h_c) = \left.\frac{\mathrm{d}^3V_s(\Delta x_m(t))}{\mathrm{d}\Delta x_m(t)^3}\right|_{\Delta x_m(t)=h_c},\\
&q = \tfrac{1}{2}\left(v_{f,\max} \pm v_{g,\max}\right).
\end{aligned} \tag{31}$$

For convenience, we set $V_s'(h_c) = V_s'$, $V_s'''(h_c) = V_s'''$. Near the critical point (h_c, a_c), let $b = qV_s'$, $\tau = (1+\varepsilon^2)\tau_c$, $\tau_c = (1 + 2TqV_s')/3qV_s'$. By eliminating the second-order and third-order terms of ε in (20), the simplified equation is further obtained

$$\begin{aligned}
&\partial_T R - g_1\partial_X^3 R + g_2\partial_X R^3\\
&\quad +\varepsilon\left(g_3\partial_X^2 R + g_4\partial_X^4 R + g_5\partial_X^2 R^3\right) = 0,
\end{aligned} \tag{32}$$

where

$$\begin{aligned}
&g_1 = -\left[b^3{\tau_c}^2 - \tfrac{1}{6}qV_s' - \tfrac{1}{2}TqV_s'\left(b + b^2\tau_c\right)\right],\\
&g_2 = -\tfrac{1}{6}qV_s''',\\
&g_3 = \tfrac{3}{2}\left(qV_s'\right)^2\tau_c,\\
&g_4 = (3b\tau_c - TqV_s')\left[-b^3{\tau_c}^2 + \tfrac{1}{6}qV_s'\right.\\
&\quad \left.+\tfrac{1}{2}TqV_s'\left(b + b^2\tau_c\right)\right] + \left(\tfrac{1}{4}b^4{\tau_c}^3 - \tfrac{1}{24}qV_s'\right.\\
&\quad \left.-\tfrac{1}{6}bTqV_s' - \tfrac{1}{4}TqV_s'b^2\tau_c\right),\\
&g_5 = \tfrac{1}{6}qV_s'''(3b\tau_c - TqV_s') - \tfrac{1}{12}qV_s''' =\\
&\quad \tfrac{1}{12}qV_s'''\left[2(3b\tau_c - TqV_s') - 1\right].
\end{aligned} \tag{33}$$

Further, (32) is transformed as follows

$$T' = g_1 T, \qquad R = \sqrt{\tfrac{g_1}{g_2}}R'. \tag{34}$$

Then, (32) can be rewritten as the following mKdV equation with correction term

$$\partial_{T'}R' - \partial_X^3 R' + \partial_X R'^3 + \varepsilon M[R'] = 0, \tag{35}$$

where $M[R'] = \sqrt{\frac{1}{g_1}}(g_3\partial_X^2 R' + g_4\partial_X^4 R' + \frac{g_1 g_5}{g_2}\partial_X^2 R'^3)$. Ignoring the correction term in (35), the kink–antikink solution of the standard modified Korteweg–de Vries (mKdV) equation can be obtained

$$R_0'(X, T') = \sqrt{c}\tanh\left(\sqrt{\frac{c}{2}}\left(X - cT'\right)\right), \tag{36}$$

where the parameter c represents the propagation velocity of kink–antikink density wave. Considering the correction term in (35), in order to obtain the wave velocity c, $R_0'(X, T')$ needs to satisfy the following conditions

$$\begin{aligned}
&\int_{-\infty}^{+\infty}\mathrm{d}X\,\frac{\sqrt{c}}{g_1 g_2}\left(g_2 g_3\partial_X^2 R' + g_2 g_4\partial_X^4 R' + g_1 g_5\partial_X^2 R'^3\right)\\
&\quad \times\tanh\left(\sqrt{\frac{c}{2}}\left(X - cT'\right)\right) = 0.
\end{aligned} \tag{37}$$

By solving the integral (37), we can get

$$c = \frac{5g_2 g_3}{2g_2 g_4 - 3g_1 g_5}. \tag{38}$$

Then, the kink–antikink density wave solution of the proposed model near the critical point (h_c, a_c) is

$$\begin{aligned}
\Delta x_m(t) &= h_c + Q\sqrt{\frac{g_1 c}{g_2}\left(\frac{\tau}{\tau_c} - 1\right)}\\
&\quad \times\left[m + \left(1 - cg_1\left(\frac{\tau}{\tau_c} - 1\right)\right)t\right],
\end{aligned} \tag{39}$$

where $Q = \tanh\sqrt{\frac{c}{2}\left(\frac{\tau}{\tau_c} - 1\right)}$.

The fluctuation amplitude A is

$$A = \sqrt{\frac{g_1 c}{g_2}\left(\frac{\tau}{\tau_c} - 1\right)}. \tag{40}$$

The kink–antikink density wave solution represents the coexisting phase, which includes the free-flow phase in the high headway region and the blocked phase in the low headway region, and the corresponding headways are $\Delta x_m(t) = h_c + A$ and $\Delta x_m(t) = h_c - A$.

5. Numerical simulation

In order to verify the theoretical analysis results, this section will carry out a numerical simulation of the proposed model under periodic boundary conditions to reveal the evolution characteristics of traffic flow density wave in its unstable region. Set the driver's sensitivity coefficient $a = 2.2$, and the initial conditions are set as follows:

$$\begin{aligned}
&\Delta x_m(0) = 4 (m \neq 50, 51),\\
&\Delta x_m(0) = 4 - 0.1 (m = 50),\\
&\Delta x_m(0) = 4 + 0.1 (m = 51).
\end{aligned} \tag{41}$$

Total number of vehicles $N = 100$, $h_c = 4$, $v_{f,\max} = 2$, $T = 0.1$. First, we randomly choose a moment to analyze the distribution of the headway under different slope angles (0°, 2°, 4°, 6°, respectively) of uphill and downhill based on the model proposed in this paper. The detailed results are shown in Fig. 4.

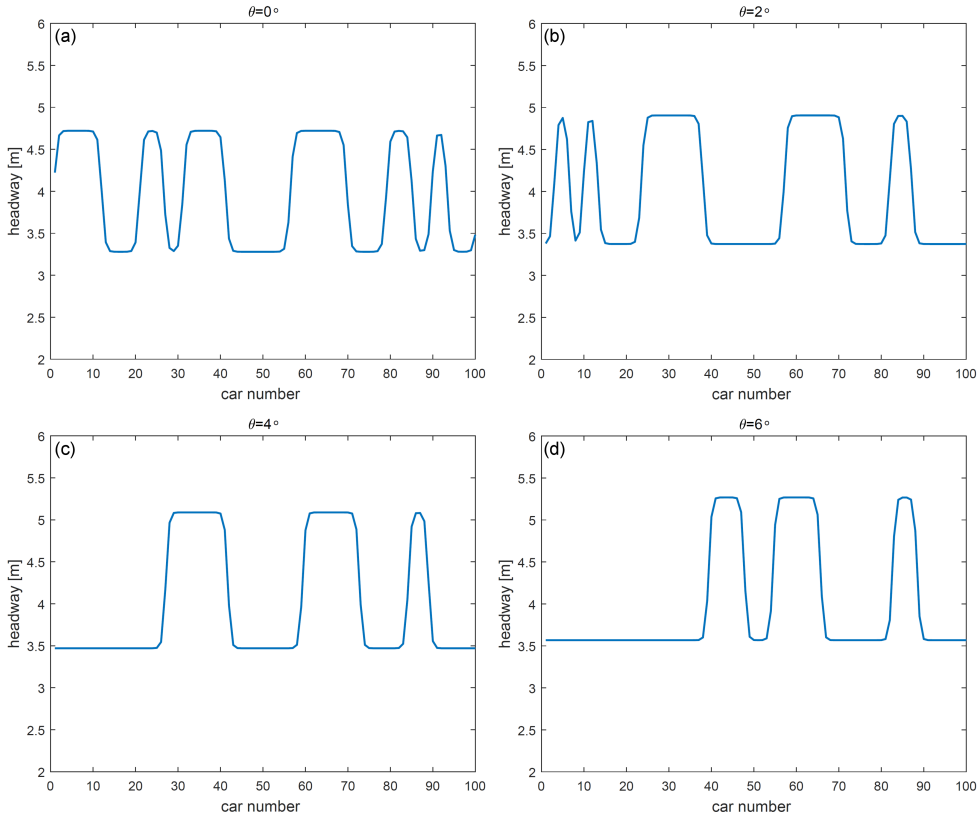

Fig. 4. Evolution curves of headway under different angles of downhill slope.

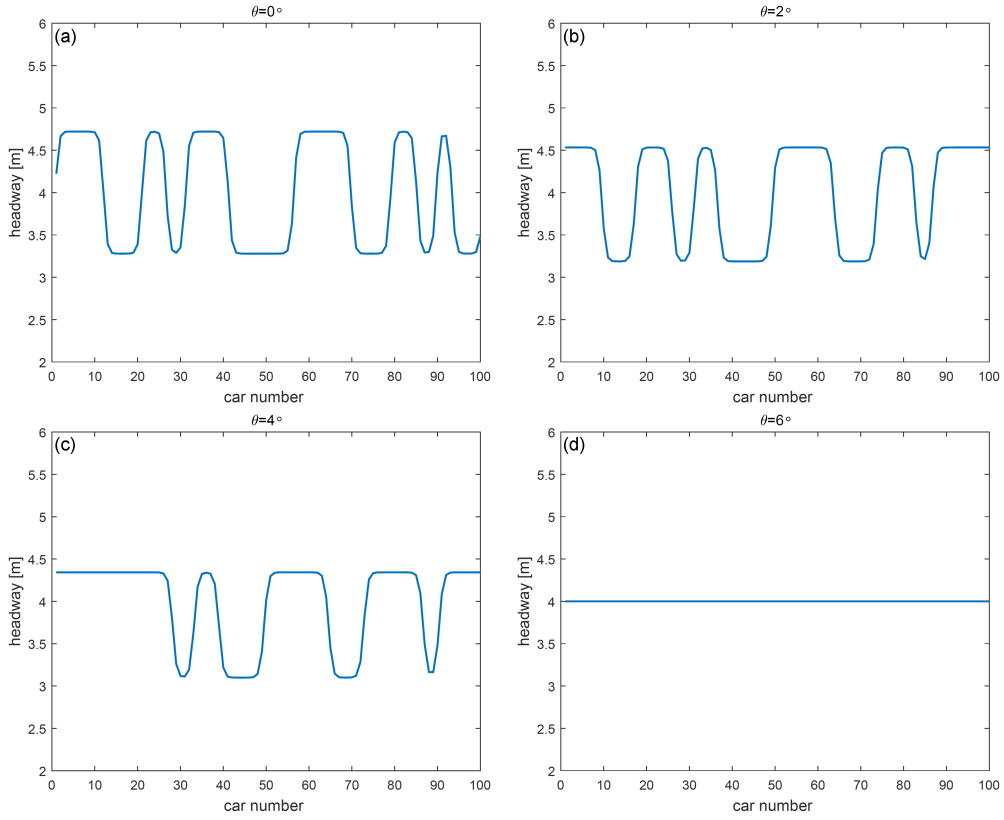

Fig. 5. Evolution curves of headway under different angles of uphill slope.

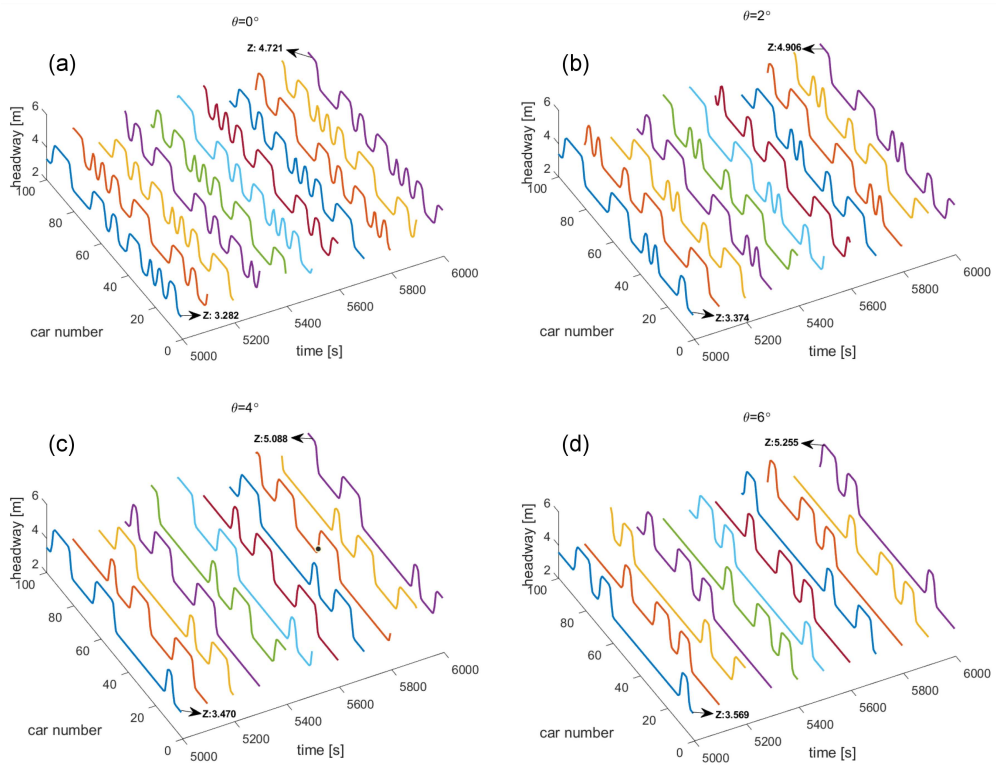

Fig. 6. Space-time evolution of headway under different angles of downhill slope.

Figure 4 shows the evolution curves of headway under different angles of the downhill slope at $t = 12000$. The horizontal coordinates in Fig. 4 indicate the number of 100 vehicles, and the vertical coordinates indicate the headway. Figure 4a, b, c, and d corresponds to the cases of the downhill angle of 0, 2, 4, and 6 degrees, respectively. Comparing these four graphs, it can be seen that the minimum headway increases from less than 3.5 m to more than 3.5 m as the downhill angle increases, while the maximum headway gradually increases from less than 5 m to more than 5 m. This indicates that when the downhill angle is small, even under the effect of the initial disturbance, the shorter headway can be maintained between vehicles, and the fluctuation amplitude is closer to the equilibrium headway of 4 m. This, in turn, indicates that the larger the downhill angle is, the less conducive to relieving traffic congestion.

Figure 5 shows the evolution curves of headway under different angles of uphill slope at $t = 12000$. Similarly to Fig. 4, Fig. 5a, b, c, and d corresponds to the cases of 0, 2, 4, and 6 degrees of uphill angle, respectively. Unlike the results in Fig. 4, the experimental results in Fig. 5 show that the headway fluctuates gradually as the uphill angle increases, and when the uphill angle is 6 degrees, the traffic flow is completely stable, and the headway is maintained at the equilibrium state of 4 m. This shows that in the uphill situation, the larger the slope, the better it is for maintaining the stability of the traffic flow. This is consistent with the previous conclusion.

In order to further represent the congestion propagation of traffic in the slope scenario, we give the space-time evolution of the headway at different slope angles. Figures 6 and 7 show the variation of the headway in the downhill and uphill scenarios over a period of time. The data tips in Fig. 6 are used to point out the values of the maximal and minimal headway in each figure. In Fig. 6, it can be seen that the stability conditions of the traffic flow are not fully satisfied under different slope conditions of the downhill slope, so the traffic flow is propagated backward in the form of a kink–antikink density wave under the initial disturbance. Meanwhile, the maximum headway becomes larger as the downhill angle increases, indicating that the steeper downhill slope is not conducive to maintaining a steady state of the traffic flow. In Fig. 7a–c, similar to Fig. 6, the traffic flow is also in an unstable state and propagates backward in the form of a kink–antikink density wave.

However, in Fig. 7d, since the system satisfies the stability condition, the traffic flow will return to a steady state after a period of time under the initial disturbance. In addition, we will also find that the maximum headway gradually decreases as the uphill angle gradually increases, and finally remains at the equilibrium state of 4 m at an angle of 6 degrees. This also shows that the steeper the uphill slope is, the more stable the flow can be.

Further, to highlight the advantages of the model in this paper, we compare the proposed model with the classical Zhu model. Figures 8 and 9 show

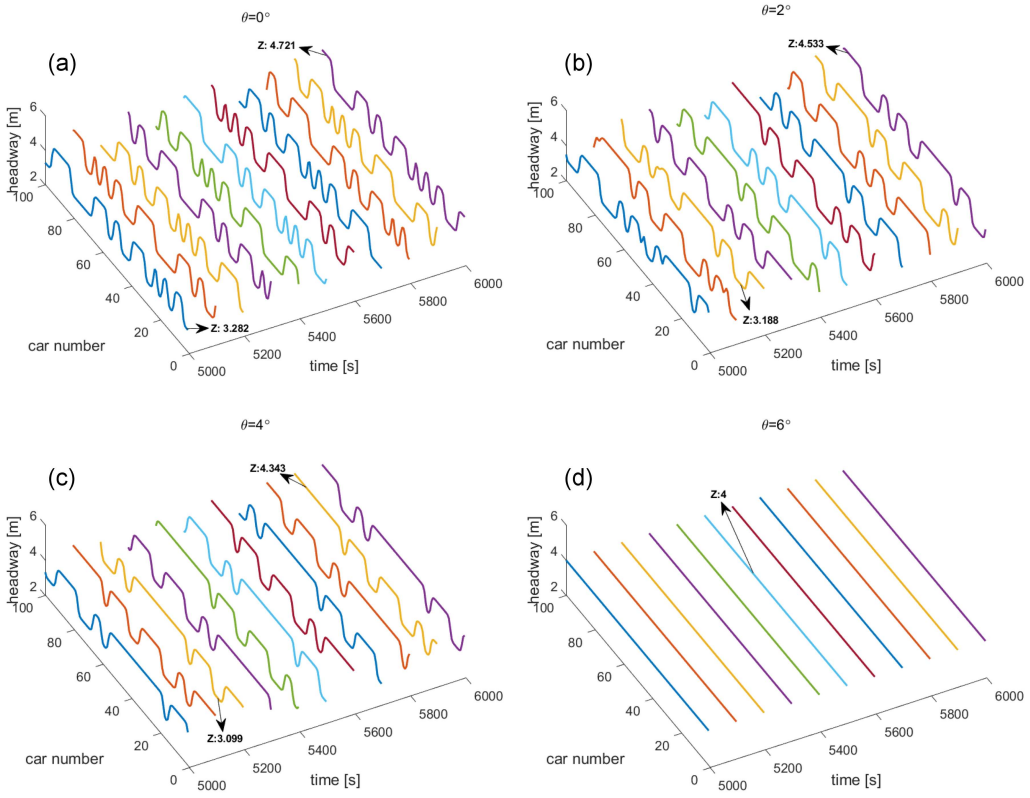

Fig. 7. Space-time evolution of headway under different angles of uphill slope.

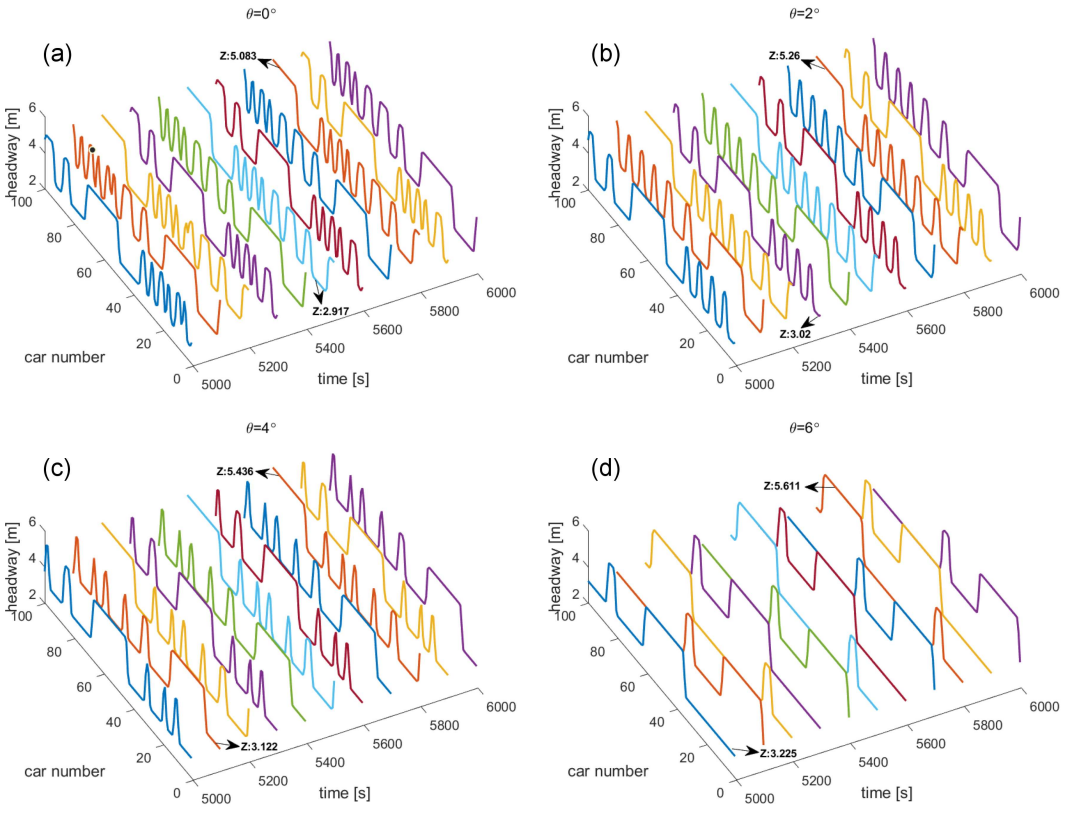

Fig. 8. Space-time evolution of headway under different angles of downhill slope (Zhu model).

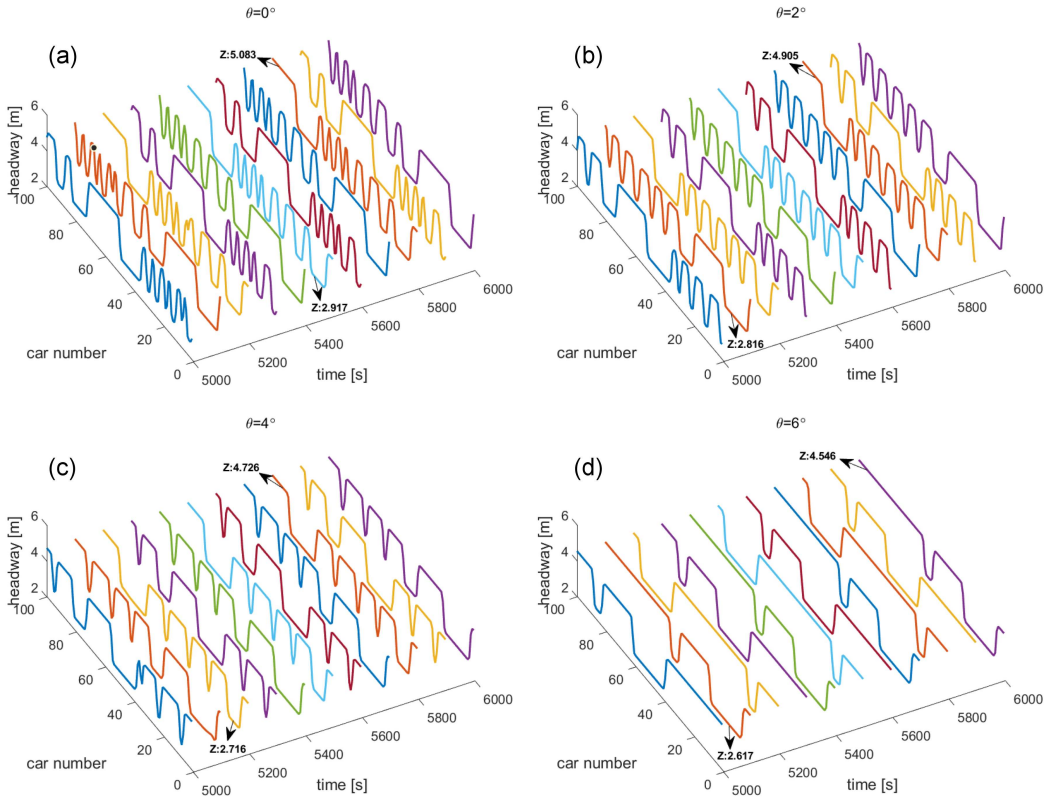

Fig. 9. Space-time evolution of headway under different angles of uphill slope (Zhu model).

the space-time evolution of the headway under the reference model at different slope angles. Comparing Figs. 8 and 6, it can be seen that our model corresponds to a lower headway for the same downhill angle, which indicates that the estimated headway information considered in the proposed model is helpful in reducing congestion and maintaining stable traffic flow.

Similarly, comparing Figs. 7 and 9, it can be seen that our model corresponds to a lower headway at the same uphill angle. What is more obvious is that our proposed model is already in a stable state when the uphill angle is 6 degrees, while the reference model is still in an unstable traffic state at that time. Therefore, this further indicates that in the slope scenario, the congestion can be effectively relieved by considering the estimated headway information so that the traffic flow can recover from the unstable state to the stable state as soon as possible.

6. Conclusions

This study introduces a new car-following model that considers estimated headway on a gradient highway. The study analyzes the effect of estimation on informed decision-making and the impact of gradient on traffic flow stability, as well as explores the relationship between estimated driving behavior on gradients and traffic congestion. Using linear stability theory, we analyze the proposed model's stability and find that estimated headway stabilizes traffic flow evolution. We then use nonlinear analysis to explore the propagation law of traffic jams near critical points. The study found that traffic jams spread through a headway wave, which is described by the mKdV equation. By conducting numerical simulations of the model with periodic boundary conditions, it was discovered that incorporating estimated headway information can improve traffic flow stability on both flat and sloped roads. The results also showed that congestion has less impact when there is a larger estimated headway. Future research should explore how lane changing affects traffic flow stability on gradients.

Acknowledgments

This work was supported by the Project funded by the China Postdoctoral Science Foundation [Grant No. 2022M710546], the Scientific and Technological Research Program of Chongqing Municipal Education Commission [Grant No. KJQN202200741].

References

[1] X. Zhang, J.Xu, Q. Liang, F. Ma, *Sustainability* **12**, 587 (2022).

[2] F. Salihu, Y.K. Demir, H.G. Demir, *Transp. Res. D* **118**, 103676 (2023).

[3] B. Goni-Ros, W.J. Schakel, A.E. Papacharalampous, M. Wang, V.L. Knoop, I. Sakata, S.P. Hoogendoorn, *Transp. Res. C* **102**, 411 (2019).

[4] D.H. Sun, G. Zhang, W.N. Liu, M. Zhao, S.L. Cheng, T. Zhou, *Nonlinear Dyn.* **86**, 269 (2016).

[5] M.U. Khan, S. Saeed, M.L. Nehdi, R. Rehan, *Appl. Sci.* **11**, 4278 (2021).

[6] N. Laurent-Brouty, G. Costeseque, P. Goatin, *SLAM J. Appl. Math.* **81**, 173 (2021).

[7] P. Zhang, Y. Xue, Y.C. Zhang, X. Wang, B.L. Cen, *Mod. Phys. Lett. B* **34**, 2050217 (2020).

[8] Z.H. Khan, T.A. Gulliver, *Eur. Transp. Res. Rev.* **10**, 1 (2018).

[9] R. Jiang, Q.-S. Wu, Z.-J. Zhu, *Appl. Math. Mech.* **23**, 409 (2002).

[10] L. Sun, A. Jafaripournimchahi, A. Kornhauser, W. Hu, *Physica A* **547**, 123829 (2020).

[11] I. Karafyllis, D. Theodosis, M. Papageorgiou, *IMA J. Math. Control Infor.* **39**, 609 (2022).

[12] Y. Xue, Y. Zhang, D. Fan, P. Zhang, H.D. He, *Nonlinear Dyn.* **95**, 3295 (2019).

[13] Y. Yuan, Z. Zhang, X.T. Yang, S. Zhe, *Transp. Res. B* **146**, 88 (2021).

[14] S.B. Li, D.N. Cao, W.X. Dang, L. Zhang, *Int. J. Mod. Phys. C* **29**, 1850014 (2018).

[15] A. Jamshidnejad, I. Papamichail, M. Papageorgiou, B. De Schutter, *Transp. Res. C* **75**, 45 (2017).

[16] V.A. Vu, G.Tan, *IEEE T. Parall. Distr.* **30**, 1691 (2019).

[17] M. Bando, K. Hasebe, A. Nakayama, A. Shibata, Y. Sugiyama, *Phys. Rev. E* **51**, 1035 (1995).

[18] D. Helbing, B. Tilch, *Phys. Rev. E* **58**, 133 (1998).

[19] M. Bando, K. Hasebe, A. Nakayama, A. Shibata, *Phys. Rev. E* **51**, 1035 (1998).

[20] L. Xing-Li, S. Tao, K. Hua,, D. Shi-Qiang, *Chin. phys. B* **17**, 3014 (2008).

[21] K. Komada, S. Masukura, T. Nagatani, *Physica A* **388**, 2880 (2009).

[22] W.X. Zhu, R.L. Yu, *Physica A* **393**, 101 (2014).

[23] X.P. Meng, L.Y. Yan, *Asian J. Control* **19**, 1844 (2017).

[24] D.H. Sun, P. Tan, D. Chen, F. Xie, L.H. Guan, *Mod. Phys. Lett. B* **32**, 1850314 (2018).

[25] Y. He, K. Mattas, R. Dona, G. Albano, B. Ciuffo, *IEEE Trans. Intell. Transp. Syst.* **23**, 13604 (2021).

[26] H. Liu, R. Cheng, H.X. Ge, *Mod. Phys. Lett. B* **35**, 2150340 (2021).

[27] C. Zhai, W.T. Wu, *Physica A* **588**, 126561 (2022).

[28] Z.H. Wang, W.X. Zhu, *Physica A* **597**, 127225 (2022).

[29] P. Zhang, Y. Xue, Y.C. Zhang, X. Wang, B.L. Cen, *Mod. Phys. Lett. B* **34**, 2050217 (2020).

[30] J. Han, X. Wang, G. Wang, *Sustainability* **14**, 8179 (2022).

[31] H. Lee, K. Kim, N. Kim, S.W. Cha, *Appl. Energy* **313**, 118460 (2022).

[32] C. Kang, Y. Qian, J. Zeng, X. Wei, *Int. J. Mod. Phys. C* **1**, 2250093 (2022).

[33] H. Liu, R. Cheng, H. Ge, *Mod. Phys. Lett. B* **35**, 2150340 (2021).

[34] A.S.M. Bakibillah, M.A.S. Kamal, C.P. Tan, *Appl. Soft. Comput.* **99**, 106875 (2021).

[35] Z. Yang, R. He, S. Zhang, J. Wu, *IET Intell. Transp. Syst.* **15**, 1478 (2021).

[36] Z. Qin, H. Shao, F. Wang, Y. Feng, L. Shen, *Sustain Energy Grids* **32**, 100877 (2022).